Rationality self-organizes beyond subjective reasonings through the coupling of brain and internal organs

Shogo Yonekura[1*†] Hoshinori Kanazawa[1†] Takuto Tsuji[1]
Atsushi Narita[1] Yasuo Kuniyoshi[1]

[1]Graduate School of Information Science and Technology, The University of Tokyo, Tokyo & 113-8656, Japan.

[*]Corresponding author. Email: {yonekura/kanazawa/kuniyosh}@isi.imi.i.u-tokyo.ac.jp

[†]These authors contributed equally to this work.

The somatic marker hypothesis proposes that internal bodily activity (IBA) is a prerequisite for rationality. However, the underlying mechanism remains unclear. First, we reveal that IBAs directly switch or lock the output of a neural circuit involved in decision-making, through human and computational studies of binocular rivalry, which is a form of perceptual decision-making. Then, through computational studies of a gambling task, we demonstrate that, if the IBA parameter is updated appropriately based on a subjective evaluation of the decision outcome, a neural network coupled with IBA can converge to rational decisions. Throughout the entire decision-making process, "Brownian ratchet" emerges, forcing unprofitable options to change while enabling rational and profitable decisions to persist. This ratchet enables intersubjective rationality to self-organize beyond subjective reasonings.

The somatic marker hypothesis (SMH), which was proposed three decades ago, suggests that information from an animal's internal organs is necessary for the brain to make rational decisions.

According to the SMH, primal and metaphysical concepts, such as good and bad or positive and negative, originate in living cells (*1*), connecting mechanical bodily processes with logical ones. These concepts reduce decisional space and bias specific options to avoid costly logical processes in the brain (*2–4*). However, the exact mechanism of the SMH remains unclear and needs to be elucidated (for the critical reviews of SMH and the recent meta-analysis study, see (*5, 6*)).

Recent research shows that internal bodily activities (IBAs) can influence brain and cognitive activity by rhythmically coupling with the brain via interoception or neuromodulation, and this rhythmic coupling affects cognitive processes such as memory and perception (*7–19*). These findings imply that there are different forms of SHM, which are based on the rhythmic coupling of the brain and internal organs rather than on the representation of subjective value information by living cells.

This paper presents a minimal neural model for SMH. First, we present evidence from human subjective studies using the binocular rivalry paradigm that rhythmic internal body activities (IBAs) can directly induce spontaneous switching in the output of a neural circuit responsible for decision-making, regardless of metaphysical value representations. Second, we demonstrate that rhythmic IBAs induce bifurcations of the decision neural circuit into decision-locking (Loc) and -switching (Sw) modes based on IBA parameters using a computational model of perceptual and general decision-making (*20*) and simple mathematical analyses. Furthermore, we demonstrate that spontaneous decision switching induced by IBAs is likely to occur at a specific phase of the IBAs. Third, we use a computational simulation of the Iowa Gambling Task (IGT) (*4*), which was designed by Bechara and Damasio, to test SMH. We demonstrate that, when coupled with IBAs, a neural decision-making circuit can enable rational decision-making without calculating the expected returns of each decision, provided that the IBAs' parameters are sequentially updated based on the subjective evaluations of decision outcomes, similar to allostasis (*21*).

Biological cells use ratchet-like mechanisms to transport molecules in a biased direction using random, symmetric thermal fluctuations. This mechanism is called a Brownian ratchet (*22, 23*). We will discuss that a somatic marker function analogously to a Brownian ratchet. Furthermore, we provide evidence that a neural circuit updated using the reward-based Hebbian rule (*24–26*) can easily exhibit irrational behavior when the subjective utility function (*27*) underestimates risk. However, emergent somatic markers can overcome the limitations of subjective reasoning

capabilities.

Cardiorespiratory influence on human perceptual alternation in binocular rivalry

In a human binocular rivalry experiment, we measured respiratory chest motion, electrocardiogram (ECG), and pupil diameter under natural breathing conditions. The phase of chest movement $\theta(t)$ corresponding to the respiratory phase, the cardiac R-wave $R(t)$, the normalized pupil diameter $d_p(t)$, the blink timing $B_l(t)$, the perceptual switching time e_p were calculated (Fig. 1-(A, B), Supplementary Text).

The likelihood of a perceptual alternation event, e_p, given the respiratory phase θ and rate (slow, normal, fast) was estimated using the Markov Chain Monte Carlo (MCMC) method (*28*) on data from 30 male participants (mean age is 25.5 with a standard deviation of 2.8). Fig. 1-(C) shows the mean and 95 % highest density interval (HDI) of the estimated likelihood function $\hat{p}(e_p|\theta)$. It is evident that $\hat{p}(e_p|\theta)$ depends on the respiration phase θ, and that the shape of $\hat{p}(e_p|\theta)$ is influenced by the respiration rate.

To confirm the statistical significance of the causal effects between IBAs and perceptual alternation, we analyzed information flow using transfer entropy (TE). In particular, TE between e_p, θ, R, d_p and B_l are estimated using a method for calculating TE between point processes (*29*). The variables $\theta(\in [0, 2\pi])$ and $d_p(\in [0, 1])$ of the nonpoint process have been converted to point processes (see Method). The heatmap in Fig. 1-(D) shows the p-values obtained from the permutation tests using the point-process TE described in Ref. (*29*). P-values less than 0.05 are indicated by red, double-underlined text. The results indicate that there is a significant flow of information from the respiratory phase and the cardiac R-wave to the perceptual alternation. See Supplementary Text and Fig.S3-S5 for the explanations of parameters and discussions of parameter sensitivity.

The vector of embedding dimensions (l_x, l_y) is a parameter that indicates how many spikes are used to compute the TE from the source process y to the target process x. The respiratory phase θ has a significant information flow with $l_y \geq 10$ with $x = 2, 3$ in slow and normal breathing rates (*30*). This implies that one cycle of breathing has a significant contribution to two and three perceptual switching events, in slow and normal breathing rates. In contrast, at fast breathing rate,

TE was only significant for $l_x < 3$. This implies that at fast breathing rate, breathing has only a short term influence.

Overall, these results demonstrate that IBAs and perceptual alternation exert a significant influence on one another, even without the reward or value information.

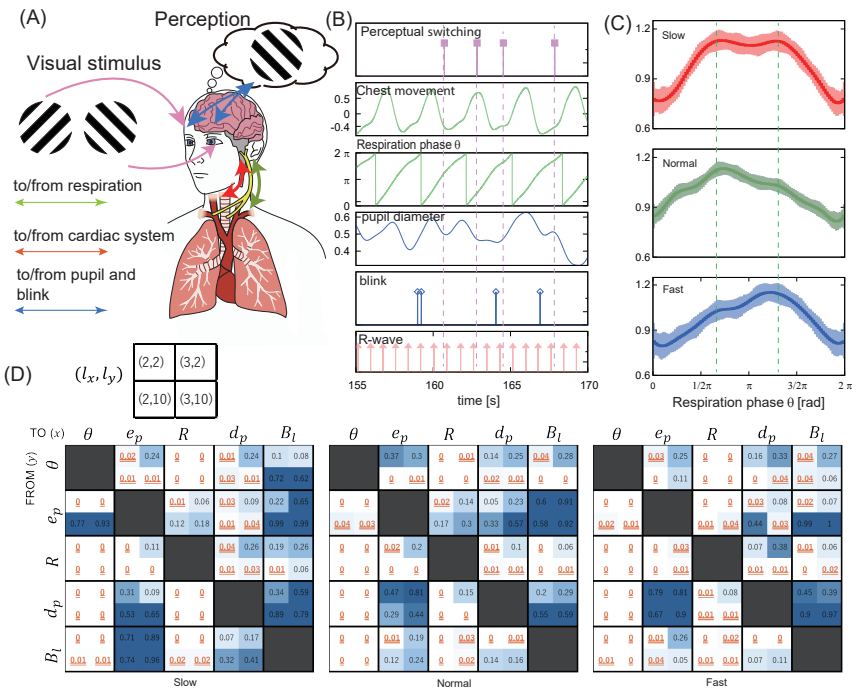

Figure 1: **Internal organs influence perceptual alternation (A)** A schematic of human experiment based on the binocular rivalry paradigm. We measured respiratory chest movement, electrocardiogram, and pupil diameters, and the timing of perceptual alternation. **(B)** A sample of the perceptual alternation timing $e_p(t)$, the phase of chest movement $\theta(t)$, the cardiac R-wave $R(t)$, the normalized pupil diameter $d_p(t)$, and the blink timing $B_l(t)$. **(C)** The estimated likelihood of perceptual alternation in human participants with respect to the respiration rate (slow, normal, fast) and the respiration phase θ, $\hat{p}(e_p|\theta)$ with the 95 % highest density interval (HDI). **(D)** Heatmaps showing the information flow from/to θ, e_p, R, d_p, and B_l. The 2×2 submatrix denotes the embedding dimension l_x, l_y used to compute TE from $y \rightarrow x$. The p-values which satisfy the condition < 0.05 are indicated by red text with a double underline.

The rhythmic activity of the internal organs induces spontaneous decision switching

It has been demonstrated that respiration entrains the overall activity of cortical neurons (*9, 15, 17*) based on the following information pathways; (a) neuromodulation of cortical neurons by the locus coeruleus, which receives respiratory information ($g(t)$) (*31–37*), and (b) the broadcast of respiratory sensory information to cortical neurons via the olfactory bulb ($A(t)$) (*9, 38, 39*) (Fig. 2-A). However, it is still unclear how rhythmic entrainment induces decision alternations. The minimal model that can account for the perceptual alternation observed in binocular rivalry is a stochastic bistable system (*40–43*). To understand the core mechanism by which IBAs influence decision-making, we therefore conducted numerical simulations and mathematical analyses using the following minimal stochastic bistable neural model (see also Fig. 2-(B), Methods):

$$\tau \frac{d\mathbf{X}}{dt} = -\mathbf{X} + f\left(g(t), \mathbf{W}\mathbf{X}\right) + A(t) + \sqrt{2D}\xi(t), \tag{1}$$

where matrix $\mathbf{X}$ denotes the membrane state of neurons, matrix $\mathbf{W}$ represents the synaptic connections, function $f(g(t), x) = 1/(1 + \exp(-g(t)\,x))$ represents the activation function of neurons, and $\sqrt{2D}\xi(t)$ denotes the Gaussian noise with the standard deviation of D. This winner-take-all (WTA) motif circuit is seen not only for perceptual alternation but also for behavioral level (*42, 44–47*). The effect of IBAs via neuromodulation is given by $g(t) = g_g \sin 2\pi f t + g_b$, and the effect via additive sensory input is given by $A(t) = A_g \sin 2\pi f t + A_b$ (Fig. 2-B, Methods). Fig. 2-(C) shows the switching of a winner neuron occurs in synchronization with the IBA-driven $g(t)$, confirming that IBAs can directly induce decision switching.

Fig. 2-(D1, D2) demonstrates that the switching of the winning neuron is likely to occur at a specific phase ϕ of IBA. Furthermore, the θ that maximizes $p(e_p|\phi)$ shifts with the IBA parameters f, g_b, g_g, A_b, and A_g.

The parameter space of IBA where decision-switching occur is linear with respect to g_b and g_g (neuromodulator bias and gain), and nonlinear with respect to A_b and A_g (sensory bias and gain) (Fig. 2-(E1–F2)).

Spontaneous flip of the feedback modes is a core mechanism of decision switching A simple mathematical analysis can demonstrate the core mechanism by which IBA influence decision-

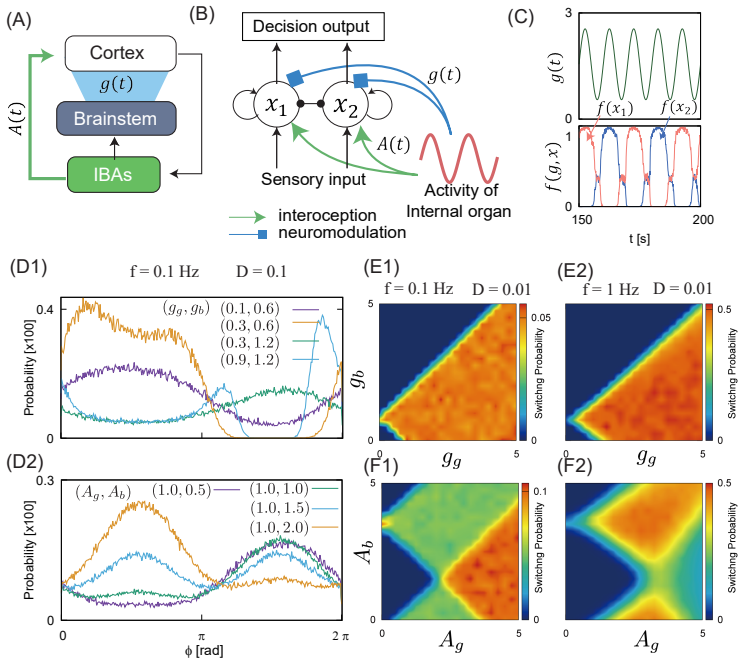

Figure 2: **Internal organs create Loc/Sw modes in a neural decision-circuit.** **(A)** Information from the animal IBA is possibly passed to cortical neurons via two pathways: neuromodulation $g(t)$ and interoceptive sensory input $A(t)$. **(B)** The simplest bistable neural model of perceptual or behavioural decision-making copled with IBA. IBA information is passed to competing neurons x_1 and x_2, via sensory input $A(t)$ and neuromodulation $g(t)$. Each competing neuron has a self-excitatory connection. **(C)** The winning neural outputs, $f(x_1)$ and $f(x_2)$, are randomly switched in a synchronised manner with periodic neuromodulation, $g(t)$. **(D1, D2)** The switching probability of winning neurons $p(e_p|\phi)$ under the influence of $g(t)$ and $A(t)$. The winning neuron tends to switch stochastically at a certain phase of $g(t)$ and $A(t)$, either at an angle of $\pi/2$ or $3\pi/2$. **(E1, E2, F1, F2)** The heatmap of switching frequency of winning neuron [Hz] in relation to neuromodulation bias (g_b) and gain (g_g), and sensory bias (A_b) and gain(A_g).

making. Taking the Taylor expansion of Eqs. 1 with $x_i \sim 0$, and computing $x_1 - x_2$, we immediately obtain the one-dimensional linear differential equation with respect to $\tilde{X} = x_1 - x_2$ as

$$\frac{d\tilde{X}}{dt} = -\tilde{X} + \frac{W_c}{4}\left(g_b + g_g \sin 2\pi f t\right)\tilde{X} + \sqrt{2D}\xi(t), \tag{2}$$

where $W_c = w_{exc} - w_{inh}$, and w_{exc} and w_{inh} are the weights for the excitatory self-coupling and the mutual inhibitory connection, respectively (see (*48*) and Methods). It is shown that the dynamics of $\tilde{X}$ is inverted from negative feedback to positive feedback based on the phase of the periodic neuromodulator, this is consistent with the results in Fig. 2-(D1). It is mathematically shown that the switching of the feedback modes occurs when $g_b > 4g_g \sin(2\pi f t)/W_c$, although large enough g_b blocks the transition of a winning neuron. The range $[-4g_g/W_c, 4g_g/W_c]$ is swept by $4g_g/W_c sin(2\pi f t)$. Therefore, the decision switching occurs around this range (Fig. 2-E1,E2)).

In contrast, the effect of interoceptive sensory input is highly nonlinear, as seen in Fig. 2-F2. The nonlinear effect of $A(t)$ to decision-making can be analyzed by using Itô's formula (*49*). If the activation gain g_b is sufficiently large, then the difference in neural outputs, $F(x_1, x_2) = f(x_1) - f(x_2)$, is described as

$$F(x_1, x_2) \sim \int_0^t \left(4g_b^2\left(x_1^2 - x_2^2\right)A(s) + H(x_1, x_2)\right)ds + Z_t + C \tag{3}$$

where $H(x_1, x_2)$ is a function of x_1 and x_2, Z_t is a noise term, C is an integral constant. It is shown that $F(x_1, x_2)$ receives the quadratic negative feedback effect $(x_2^2 - x_1^2)$ when $A(t)$ is in the phase $[0, \pi]$ and similarly, the positive feedback effect in the phase $[\pi, 2\pi]$. For the detailed derivation and explanation of Eq. 3, see Supplementary Text.

Rationality self-organizes

In IGT, an agent repeatedly draws a card from a bad (BD) or good (GD) deck, where the expected value of each deck is unknown. BD is designed to generate a high random score in the short term. However, the expected return is negative, so selecting BDs results in long-term losses. In contrast, GD is configured to produce only a small random score, but it has a positive expected return. Thus, choosing GDs leads to long-term profits. The score R_n, that an agent receives at the n-th decision is designed as follows: $R_n = -25 - r_0 + 375\xi_n$ for BD and $R_n = 25 - r_0 + 75\xi_n$ for GD, where ξ_n is a random number generated from a normal distribution.

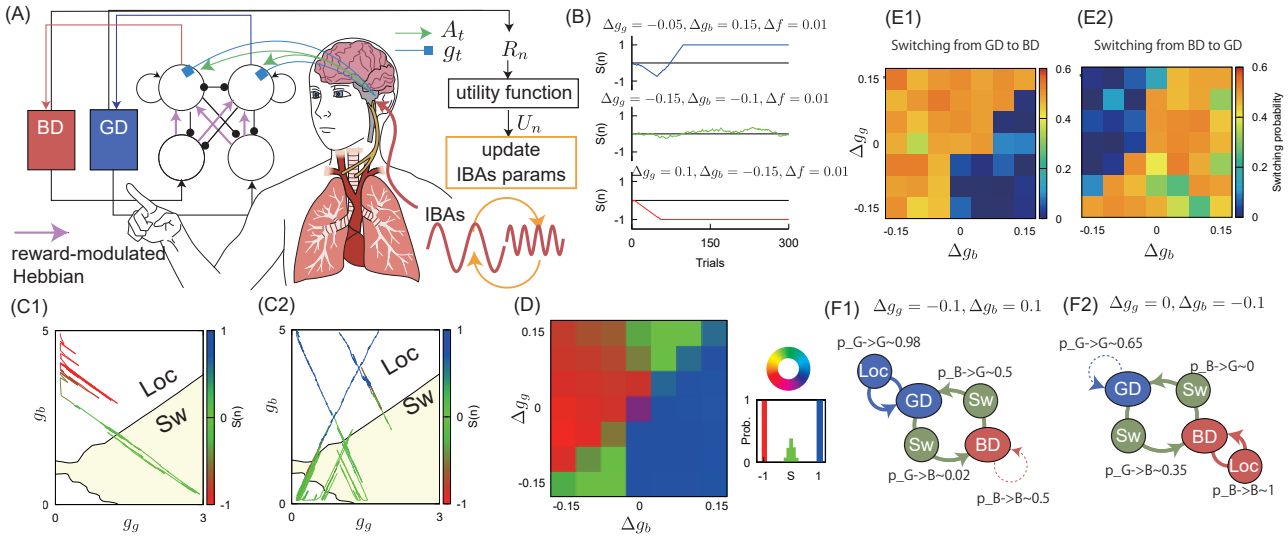

Figure 3: **A minimal model of SMH in IGT (A)** A schematic diagram of the task and a computational SMH model. BD is bad deck and GD is good deck. The decisional neural circuit repeatedly chose one of the decks and received the score R_n. R_n is evaluated internally, and IBAs are updated based on U_n. The decision neural circuit is basically the same with Fig. 2 but has top-down inhibitory connection, which is called "evidence cut-off" (*42*). The task performance is measured by $S(n)$, which represents how often the agent selected GD. **(B)** Trajectories of $S(n)$ when the agent successfully converged to GD $S(\infty) = 1$, and BD $S(\infty) = -1$, or keep wondering $S(\infty) \sim 0$. **(C1, C2)** Trajectories of $g(t)$ for $S(\infty) = -1$ **(C1)** and $S(\infty) = 1$ **(C2)** are superimposed on the phase diagram of Loc and Sw. **(D)** The influence of the mapping functions of $U_n \rightarrow \Delta g_g, \Delta g_b$. We computed the histogram of $S(\infty)$, i.e., $p(S(\infty) = x)$ for each parameter set $(\Delta g_b, \Delta g_g)$, and colored it according to the ratio of red for $p(S(\infty) = -1)$, green for $p(S(\infty) = 0)$, and blue for $p(S(\infty) = 1)$. **(E1, E2)** The transition probabilities from GD to BD and from BD to GD, respectively. **(F1, F2)** Understanding the entire system using finite state machines; the switching probability from GD $\rightarrow$ GD via Loc mode, GD $\rightarrow$ BD via Sw mode are measured using several typical parameters.

We use the measure $S(n)$, which denotes how often an agent selects GD; If the agent consistently chooses GD, $S(n)$ converges to 1; if the agent consistently chooses BD, $S(n)$ converges to -1; and if the agent consistently switches between GD and BD, $S(n) \sim 0$ (Fig. 3-A, Methods).

We assumed that the neural gain is influenced by rhythmic IBAs as follows: $g = g_g \sin(2\pi f t) + g_b$. The agent evaluates the outcome of the nth decision, R_n, using the internal utility function $U_n = U(R_n)$; $U(R) = R$ for $R > 0$ and $-|R|^\beta$ for $R < 0$ ($\beta < 1$ means risk underestimation). After every decision, the IBA parameters are updated in a linear manner based on U_n as follows: $z(n+1) = (1+\zeta_n)z(n) + \Delta_z(\lambda U_n + \eta_n)$, where z denotes either g_g, g_b, or f, λ is a scaling factor, and η and ζ are small Gaussian noise (Methods).

Fig. 3-(B) show that the agent can reach a rational decision and converge through the IBA-induced spontaneous and implicit transitions between Loc and Sw (Fig. 3-C1, C2). Furthermore, the top panel in Fig. 3-(B) shows that the agent successfully performed spontaneous reversal learning, which is believed to be a key function of somatic markers in healthy persons; the agent first selected BD because it provided large rewards for the first ~ 50 trials. However, BD soon started to return large negative scores, and the agent successfully changed its decision and converged on GD.

Fig. 3-(D) shows that metalearning, i.e., an appropriate configuration of Δ_z (i.e., Δg_g or Δg_b) by a brain is necessary for the occurrence of rationality emergence. If Δz is not adequate, the system is trapped to irrational behaviors (the bottom panel of Fig. 3-B, and C1).

The overall behavior of the coupled sytem is described as a finite state machine (Fig. 3-E, F); if $U_n < 0$ and $U_n > 0$ are mapped to IBA's parameter update toward Loc and SW regions, respectively, then, the decision of BD is stabilized in this overall process because BD returns negative outcome in average. In contrast, if $U_n < 0$ and $U_n > 0$ are mapped to IBA's parameter update toward SW and Loc modes, respectively, then, the decision is locked to GD in this overall process because GD returns positive outcome in average. It is important to note that the agent neither knows nor calculates the expected values of BD and GD.

Fig. 4 shows that for the asymmetric profit-loss stucture of IGT ($r_0 \neq 0$), the optimal configuration of Δ_z to spontaneously generate rational decisions varies. It should be noted that the reward-modulated Hebbian learning rule (*24–26*), which is an implementation of reinforcement learning based on Hebbian rule, is very weak to risk-underestimation, and the learning process

easily corrups for $\beta < 1$. Despite the distorted utility function, SMH succeeds in making rational decisions, though a precise and flexible configuration of Δ_z seems to be required.

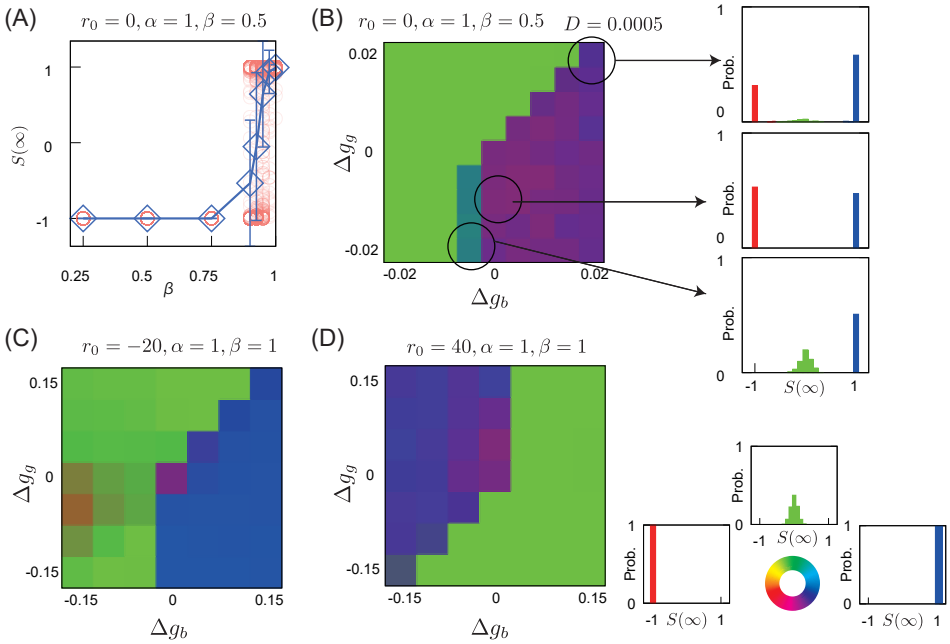

Figure 4: **Reward-based Hebbian learing versus IBA-supported decision-making under distorted, asymmetric utility function** U_n **(A)** Limitation of reward-based Hebbian learning when the utiliy function underestimates risk ($\beta < 1$), the reinforcement learning easily drops to risky option; $S(\infty) = -1$. **(B)** SMH can find rational decision $S(\infty) = 1$ even with the highly risk underestimation $\beta = 0.5$, although such parameter region is narrow $\Delta - 0.005 \leq g_b \leq 0$ and $\Delta g_g < 0$. **(C)** For asymmetric bias $r_0 = -20$ (the expected score of GD is large, i.e., = 45, whereas the expected score of BD is = −5), behaviors for $S(\infty) = -1$ tends to disappear and most of behaviors converges to $S(\infty)0$ or 1. **(D)** For $r_0 = 40$, which means that both BD and GD return negative score in average, the parameter regions which yield the selection of GD are inverted compared to **(C)** and Fig. 3-D.

Discussion

Intersubjective rationality beyond subjective reasonings Fig. 4-(A) show the surprising results that reward-modulated Hebbian learning—which we believe is a simple, neural-level implementation of the value-based reasoning process, corresponding to Bayesian computation (*24–26*)—cannot

produce rational decision-making when the internal evaluative utility function is even slightly biased toward underestimating risk. This result highlights a serious issue: while a learning process based on an subjective evaluation function is reasonable from the system's viewpoint, it is considered irrational by an outside observer. Therefore, rationality cannot be achieved by the local learning rule in the brain alone.

To correct distorted subjective evaluations and establish a "rational" decision-making process aligned with external consensus, one needs another mechanism which can share information with an "external" existence. (This external existence could be another person or society, for example). Our results suggest that flexible and heuristic maps of subjective evaluations onto internal organs (Fig. 4-B, C, D) can sufficiently correct these distorted evaluations, yielding self-organization of rationality that aligns with external consensus. Within the original SMH framework, the ventromedial prefrontal cortex (vmPFC) (*2, 3*) must be responsible for the metacognitive, heuristic mapping of subjective evaluations onto internal organs based on allostatic functions (*21*).

Somatic marker as behavioral Brownian ratchet We have demonstrated that SMH functions analogously to a Brownian ratchet (*22, 23*), as follows. Internal organs create the Loc and Sw modes of a decisional neural circuit in a brain. The modes bifurcate based on IBAs' parameters. The brain controls rhythmic IBAs based on decision outcomes and indirectly controls the switching and locking modes of a decision circuit. In this entire decision-making loop, the brain determines the direction of the ratchet by mapping the outcome of the decision onto the parameters of the internal organs. Once the brain has successfully configured the direction of the ratchet, the emergent Brownian ratchet spontaneously eliminates irrational and unprofitable options, allowing rational, profitable ones to persist.

Somatic markers must exist within the entire interaction loop of a brain, a body, and an environment The internal organs in our model do not encode the expected value of each specific option unlike the original SMH that posits living cells encode metaphysical value information, though the cumulative total score from all decision-making trials is encoded as IBA parameters. Our results are consistent with research demonstrating that changes in IBA correlated with feedback on decision outcomes are important for IGT performance (*6*). Furthermore, our results suggest that

a Brownian ratchet emerged throughout the entire decision-making process, serving as the basis for rational decision-making by overwriting the subjective evaluation. It is reasonable to conclude that the somatic marker that aids in the formation of intersubjective rationality does not originate from independent living cells, but rather from the entire intersubjective decision-making loop, at least in our model.

Conclusion

The present study showed that perceptual decisions in human binocular rivalry are influenced by the activity of internal organs. Through computational and mathematical analysis, we showed that internal organs can bifurcate the decision-making output in a brain to lock and switch modes. Through computational simulations of the IGT, we demonstrated that decision-making agents who receive rhythmic information from internal organs can make rational decisions without knowing or estimating the value of decision outcomes. We demonstrated that reward-based Hebbian learning can be easily corrupted by biased subjective reasoning and evaluation systems that underestimate risk. However, coupling the brain with the internal organs can enable rational decision-making. We revealed a core mechanism of SMH: the rhythmic activity of the internal organs bridges subjective reasoning and intersubjective rationality.

References and Notes

1. A. R. Damasio, ed., *Looking for Spinoza* (Mariner Book, New York, USA) (2003).

2. A. R. Damasio, ed., *Descartes' Error* (Putnam Adult, New York, USA) (1994).

3. A. R. Damasio, The somatic marker hypothesis and the possible functions of the prefrontal cortex. *Phil. Trans. R. Soc. B* **351** (1346), 1413–1420 (1996).

4. A. Bechara, A. R. Damasio, The somatic marker hypothesis: A neural theory of economic decision. *Game Econ. Behav.* **52**, 336–372 (2005).

5. B. D. Dunn, T. Dalgleish, A. D. Lawrence, The somatic marker hypothesis: A critical evaluation. *Neurosci. Biobehav. Rev.* **30**, 239–271 (2005).

6. B. Simonovic, E. Stupple, M. Gale, D. Sheffield, Sweating the small stuff: A meta-analysis of skin conductance on the Iowa gambling task. *Cogn Affect Behav Neurosci* **19**, 1097–1112 (2019).

7. S. N. Garfinkel, *et al.*, Fear from the heart: Sensitivity to fear stimuli depends on individual heartbeats. *J Neurosci* **34** (19), 6573–6582 (2014).

8. S. N. Garfinkel, H. D. Critchley, Threat and the body: How the heart supports fear processing. *Trends Cogn. Sci.* **20** (1), 34–46 (2016).

9. C. Zelano, *et al.*, Nasal respiration entrains human limbic oscillations and modulates cognitive function. *J. Neuroscience* **36** (49), 12448–12467 (2016).

10. J. F. Thayer, A. L. Hansen, E. Saus-Rose, B. H. Johnsen, Heart rate variability, prefrontal neural function, and cognitive performance: the neurovisceral integration perspective on self-regulation, adaptation, and health. *Ann. Behav. Med.* **37**, 141–153 (2009).

11. I. Rebollo, A.-D. Devauchelle, B. Béranger, C. Tallon-Baudry, Stomach-brain synchrony reveals a novel delayed-connectivity resting-state network in humans. *eLife* **7**, e33321 (2018).

12. N. Wolpert, C. Tallon-Baudry, Coupling between the phase of a neural oscillation or bodily rhythm with behavior: Evaluation of different statistical procedures. *NeuroImage* **236**, 118050 (2021).

13. H.-D. Park, O. Blanke, Heartbeat-evoked cortical responses: Underlying mechanisms, functional roles, and methodological considerations. *NeuroImage* **197**, 502–511 (2019).

14. A. M. Herman, M. Tsakiris, Feeling in control: The role of cardiac timing in the sense of agency. *Affect. Sci.* **1**, 155–171 (2020).

15. D. S. Kluger, E. Lalestrieri, N. A. Busch, J. Gross, Respiration aligns perception with neural excitability. *eLife* **10**, e70907 (2021).

16. A. Galvez-Pol, P. Virdee, J. Villacampa, J. Kilner, Active tactile discrimination is coupled with and modulated by the cardiac cycle. *eLife* **11**, e78126 (2022).

17. S. Ashhad, K. Kam, C. A. D. Negro, J. L. Feldman, Breathing rhythm and pattern and their influence on emotion. *Annu Rev Neurosci* **45**, 223–2247 (2022).

18. T. Engelen, M. Solcà, C. Tallon-Baudry, Interoceptive rhythms in the brain. *Nat Neurosci* **26**, 1670–1684 (2023).

19. J. P. Veillette, F. Gao, H. C. Nusbaum, Cardiac afferent signals can facilitate visual dominance in binocular rivalry. *eLife* **13**, RP95599 (2024).

20. Binocular rivalry was chosen as the target phenomenon for decision-making because it has been demonstrated that the same winner-take-all neural circuitry is responsible for both behavioral and perceptual decision-making, independent of reward or value information. This motif circuit corresponds to decisions such as whether to go or not, or whether to move left or right (*42, 44–47*).

21. P. Sterling, Allostasis: a model of predictive regulation. *Physiol. Behav.* **106** (1), 5–15 (2012).

22. R. P. Feynman, R. B. Leighton, M. Sands, The Feynman Lectures on Physics (Addison-Wesley), chap. 46 (1963).

23. R. D. Astumian, Thermodynamics and kinetics of a Brownian motor. *Science* **276**, 917–922 (1997).

24. R. Legenstein, S. M. Chase, A. B. Schwartz, W. Maass, A reward-modulated Hebbian learning rule can explain experimentally observed network reorganization in a brain control task. *J. Neurosci.* **30** (25), 8400–8410 (2010).

25. B. Nessler, M. Pfeiffer, L. Buesing, W. Maass, Bayesian computation emerges in generic cortical microcircuits through spike-timing-dependent plasticity. *PLOS Computat Biol* **9** (4), e1003037 (2013).

26. S. Klampfl, W. Maass, Emergence of dynamic memory traces in cortical microcircuit models through STDP. *J. Neurosci.* **33** (28), 11515–11529 (2013).

27. J. von Neumann, O. Morgenstern, eds., *Theory of Games and Economic Behavior* (Princeton University Press, NJ, USA) (1944).

28. J. Cook, Splines, in *PyMC examples*, P. Team, Ed., doi:10.5281/zenodo.5654871.

29. D. P. Shorten, R. E. Spinney, J. T. Lizier, Estimating transfer entropy in continuous time between neural spike trains or other event-based data. *PLOS Comput Biol* **17** (4), e1008054 (2021).

30. The point process Y corresponding to the respiration phase θ with $I_y = 10$ denotes one cycle of respiration; for we computed the point process by dividing the parameter space $\theta : [0, 2\pi]$ into 10 subspaces. See Supplementary Text for more details.

31. M. C. Melnychuk, *et al.*, Coupling of respiration and attention via the locus coeruleus: Effects of meditation and pranayama. *Psychophysiolgy* **55** (9), e13091 (2017).

32. T. Poppa, A. Bechara, The somatic marker hypothesis: revisiting the role of the 'body-loop' in decision-making. *Curr. Opin. Behav. Sci.* **19**, 61–66 (2018).

33. L. T. Lopes, *et al.*, Anatomical and functional connections between the locus coeruleus and the nucleus tractus solitarius in neonatal rats. *Neuroscience* **324**, 446–468 (2016).

34. M. C. Quintero, R. W. Putnam, J. M. Cordovez, Theoretical perspectives on central chemosensitivity: CO_2/H_2-sensitive neurons in the locus coeruleus. *PLoS Comput Biol* **13** (12), e1005853 (2017).

35. D. de Carvalho, *et al.*, Participation of locus coeruleus in breathing control in female rats. *Respiratory Physiol. & Neurobiol.* **245**, 29–36 (2017).

36. Y. Oyamada, D. Ballantyne, K. Mückenhoff, P. Scheid, Respiration-modulated membrane potential and chemosensitivity of locus coeruleus neurones in the in vitro brainstem-spinal cord of the neonatal rat. *J. Physiol.* **513** (2), 381–398 (1998).

37. K. Yackle, *et al.*, Breathing control center neurons that promote arousal in mice. *Science* **355**, 1411–1415 (2017).

38. D. H. Heck, *et al.*, Breathing as a fundamental rhythm of brain function. *Front. Neural Circuits* **10**, Article 115 (2017).

39. L. M. Kay, P. Lazzara, How global are olfactory bulb oscillations ? *J. Neurophysiol* **104** (3), 1768–1773 (2010).

40. Y.-J. Kim, M. Grabowecky, S. Suzuki, Stochastic resonance in binocular rivalry. *Vision Res* **46**, 392–406 (2005).

41. M. T. Cuello, A. Drew, A. S. S. Jose, L. M. Fernández, S. Soto-Faraco, Alpha fluctuations regulate the accrual of visual information to awareness. *Cortex* **147**, 58–71 (2022).

42. R. Cao, A. Pastukhov, S. Aleshin, M. Mattia, J. Braun, Binocular rivalry reveals an out-of-equilibrium neural dynamics suited for decision-making. *eLife* **10**, e61581 (2021).

43. A. W. Freeman, Multistage model for binocular rivalry. *J Neurophysiol* **94** (6), 4412–4420 (2005).

44. J. W. Kable, P. W. Glimcher, The neurobiology of decision: Consensus and controversy. *Neuron* **63** (6), 733–745 (2009).

45. A. T. Kuan, *et al.*, Synaptic wiring motifs in posterior parietal cortex support decision-making. *Nature* **627**, 367–373 (2024).

46. M. Usher, J. D. Cohen, D. Servan-Schreiber, J. Rajkowski, G. Aston-Jones, The role of locus coeruleus in the regulation of cognitive performance. *Science* **283** (5401), 549–554 (1999).

47. G. Aston-Jones, J. D. Cohen, An integrative theory of locus coeruleus-norepinephrine function: Adaptive gain and optimal performance. *Annu. Rev. Neurosci.* **28**, 403–450 (2005).

48. The time-constant τ in Eq.1 can be removed by applying adequate scaling of $\mathbf{X}$ and t, and we have $d\hat{\mathbf{X}}/d\hat{t} = -\hat{\mathbf{X}} + f(\hat{\mathbf{W}}\hat{\mathbf{X}}) + \hat{A}(\hat{t}) + \hat{D}\xi(\hat{t})$, where $\hat{\cdot}$ represent the scaled variable.

49. K. Itô, On a formula concerning stochastic differentials. *Nagoya Math. J.* **3**, 55–65 (1951).

50. A. L. Goldberger, *et al.*, PhysioBank, PhysioToolkit, and PhysioNet: components of a new research resource for complex physiologic signals. *Circulation* **101** (23), e215–e220 (2000).

Acknowledgments

Funding: This study was partially funded by Toyota Central R&D Labs., Inc., Chair for Frontier AI Education of the Next Generation AI Research Center, The University of Tokyo, and JSPS KAKENHI Grant Number JP 25H00448.

Author contributions: Conceptualization, S. Y., A. N., H. K. and Y. K.; methodology, S. Y., A.N., H. K., and T. T.; human data curation, H. K. and A. N.; formal analysis, S. Y., A. N., and H. K.; funding acquisition; Y. K.; project administration, Y. K.; resources, Y. K. and H. K.; software and simulation, S. Y., T. T., and A. N.; validation, H. K., T. T., and Y.K.; writing and reviewing; S. Y., H. K., and Y. K.; All authors above read and agreed to the published version of the manuscript.

Competing interests: There are no competing interests to declare.

Ethics approval and consent to participate The binocular rivalry experiments described in this paper was approved by the ethics committees of our institute. All participant for the binocular rivalry experiments signed an informed consent statement.

Data and materials availability: All data and codes used in this paper is downlodable at `https://osf.io/xv34g/?view_only=a151c4fb80d74b3a84523e64b741491a`

Supplementary materials

Materials and Methods

Supplementary Text

Figs. S1 to S5

Tables S1

References *(7-50)*